Proof of principle of a purine D–A–D' ligand based ratiometric chemical sensor harnessing complexation induced intermolecular PET

Justina Jovaisaite, Dace Cīrule, Andris Jeminejs, Irina Novosjolova, Māris Turks, Paulius Baronas, Regimantas Komskis, Sigitas Tumkevicius, Gediminas Jonusauskas, Saulius Jursenas

Proof of principle of a purine D–A–D′ ligand based ratiometric chemical sensor harnessing complexation induced intermolecular PET†

Justina Jovaisaite, *[a] Dace Cīrule,[b] Andris Jeminejs,[b] Irina Novosjolova,[b] Māris Turks, [b] Paulius Baronas, [a] Regimantas Komskis,[a] Sigitas Tumkevicius, [a] Gediminas Jonusauskas *[c] and Saulius Jursenas[a]

A comprehensive photophysical study of a series of purines, doubly decorated at C2 and C6 positions with identical fragments ranging from electron acceptor to donor groups of different strengths, is presented. The asymmetry of substitutions creates a unique molecular D–A–D′ structure possessing two independent electronic charge transfer (CT) systems attributed to each fragment and exhibiting dual-band fluorescence. Moreover, the inherent property of coordination of metal ions by purines was enriched due to a presence of nearby triazoles used as spacers for donor or acceptor fragments. New molecules present a bidentate coordination mode, which makes the assembly of several ligands with one metal cation possible. This property was exploited to create a new concept of a ratiometric chemical fluorescence sensor involving the photoinduced electron transfer between branches of different ligands as a mechanism of fluorescence modulation.

Introduction

Organic π-conjugated systems with electron accepting cores coupled with electron donating functional groups are generally known as push–pull materials that have been of high interest for years due to their charge transfer (CT) character, tuneable optical properties and HOMO–LUMO gap, and non-linear optical response.[1] The donor–acceptor–donor′ (D–A–D′) type of push–pull compounds stands out with their uniqueness as two different electron donating parts are combined, allowing both to maintain the symmetry of molecules or to realize asymmetric structures. A wide variety of possible D–A–D′ chemical structures and configurations provides an opportunity to tune energy levels and molecular geometries that further assist in the development of organic solution based as well as soft and semiconducting materials. The latter strategy has already found its application in the development of organic solar cells,[2–5] as well as third generation organic light emitting diodes (OLEDs).[6–8] Furthermore, the D–A–D′ structure based intramolecular chemical sensors have been reported for multimodal detection of metal cations[9] or acids.[10]

The electron donating parts such as anisole and dimethylaniline are considered to be general for push–pull systems[1] and may be selected based on their strength. Purines, on the other hand, are known to be ambipolar;[11] however, using them as electron accepting units may provide several advantages.

Purines as nitrogen heterocycles are starting materials widely available in the natural product pool and are readily accessible for chemical modifications that can alter their photophysical properties dramatically. The electron donating functional groups may be coupled at the C2, C6 or C8 positions of the purine core. Some of the desired optical properties of the purine push–pull derivatives have been achieved due to the progress in synthetic methods and their integrity.[12,13] For instance, the azole-type substituents at the C2 and (or) at the C6 position of the purine core enabled reaching fluorescence quantum yields (QYs) of around 60%[14] (in the case of 7-deazapurines, similarly substituted compounds exhibit more than 70% of QYs[14–16]) while by complementing typical donor groups at C2 and C6 of the purine by a substituent at C8, fluorescence quantum yields of near unity were easily achieved.[17] In addition to high fluorescence quantum yields, more advantages of push–pull purine systems can be realized and successfully applied. The purine derivatives have already been demonstrated as emitters in OLEDs,[18–20] as pH[21] sensors

[a] Institute of Photonics and Nanotechnology, Faculty of Physics, Vilnius University, Sauletekis Av. 3, LT-10222 Vilnius, Lithuania. E-mail: justina.jovaisaite@ff.vu.lt
[b] Institute of Technology of Organic Chemistry, Faculty of Materials Science and Applied Chemistry, Riga Technical University, Valdena Str. 3, LV-1048 Riga, Latvia
[c] Laboratoire Ondes et Matière d'Aquitaine, Bordeaux University, UMR CNRS 5798, 351 Cours de la Libération, 33405 Talence, France.
E-mail: gediminas.jonusauskas@u-bordeaux.fr

or even as imaging tools for cell compartments[22] and their environment.[23] Additionally, the purine derivatives are natural-like molecules that can be more easily recognized by cells.[14]

During the last decade a few examples of purines bearing traditional complexing structures like crown ethers,[24] pincer forming substituents[25] and salicyl-imine side chains[22] have been reported and applied as metal ion sensors. Alternatively, derivatives containing an external C8-complexing arm which works in tandem with the purine N7 have been developed.[26,27] To the best of our knowledge, there are only a few recent examples of the purine-based metal ion sensors that make use of both C6-substitent and the purine N7.[28–30]

Herein, we present the design, synthesis and photophysical properties of four 2,6-bis-(1,2,3-triazol-1-yl)purine derivatives (see Synthesis and product characterization in the ESI†).[31] Our design extends the use of the metal ion complexation mode between a ligand attached to C6 and the N7 intrinsic for the purine ring. Moreover, with the 2,6-bis-substituted systems we demonstrate the utility of complex forming ligands at the purine C2 position for the first time. The investigated compounds bear an electron accepting methyl carboxylate (compound **1**) or an electron donating phenyl ring (**2**),[32,33] and 4-methoxyphenyl (**3**) or 4-*N*,*N*-dimethylaminophenyl (**4**) functional groups at the C4 position of each triazole ring (Fig. 1).

The combination of two chemically identical electron donating branches at the purine C2 and C6 positions (compounds **2**, **3** and **4**), allowed the creation of unique donor–acceptor–donor′ (D–A–D′) systems with two distinct electron transitions from each of the electron donating branches. The latter molecular design results in dual fluorescence in polar aprotic solvents that is altered by the strength of the electron donating properties of the substituents. The close proximity of D–A–D′ molecules upon complexation with metal ions enables the intermolecular interbranch photoinduced electron transfer (PET) with subsequent complete quenching of a blue side band of dual fluorescence. This allows demonstrating a new concept of a ratiometric fluorescence sensor.

Results and discussion

Independent CT states of D–A–D′ purines

The photophysical characterization of each compound was performed in aprotic solvents of different polarities (ethyl acetate (EA), dimethoxyethane (DME) and acetonitrile (ACN)) and summarized in Table 1 The representative absorption and fluorescence spectra in ACN are given in Fig. 2a and b.

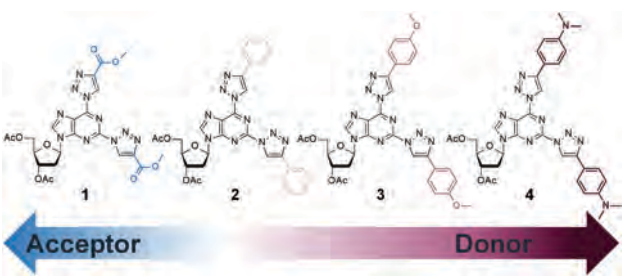

Fig. 1 Chemical structure of bis-triazolyl-purine nucleoside derivatives with electron accepting (**1**) and electron donating (**2**, **3**, **4**) substituents.

The absorption spectra in ACN of all studied derivatives have two intense UV-blue bands, which in the case of **1** have their maxima at around 250 nm and 300 nm, typical of other purine analogues, substituted at C2 and C6 or at C8 positions.[34,35] Once the conjugation is expanded by the addition of electron donating functional groups, the lowest absorption band gradually red shifts (from 298 nm (**1**) to 364 nm (**4**)).

As revealed by TD-DFT modelling , the lowest energy transitions (for compounds **2**, **3** and **4**) are of the charge transfer (CT) nature related to both electron donating substituents and bis-triazolyl-purine as an electron acceptor. The schematic view of HOMO−1, HOMO, LUMO, LUMO+1 energies for each compound are given in the Fig. 2a inset . The analysis of molecular orbitals shows that HOMO−1 and HOMO correspond to substituents coupled at the purine C2 and C6 positions, respectively, and are energetically separated by *ca.* 130 meV. Intense higher-energy absorption bands (for compounds **2**, **3** and **4** peaking from 244 nm to 290 nm) consist of several transitions, including strong locally excited (LE) states in each of electron donating branches, the purine core itself and higher energy CT transitions.

More pronounced changes are observed in the fluorescence spectra (Fig. 2b). Compound **1** has the blue LE fluorescence peaking at 358 nm, which, as expected, does not depend on the polarity of the surrounding media . However, in accordance with the CT nature of the lowest absorption states of **2**, **3** and **4**, the emission spectra in ACN are broadened and strongly bathochromically shifted (from 358 nm (**1**) to 653 nm (**4**)),

Table 1 Steady-state spectroscopic data for compounds **1–4** obtained in ethyl acetate (EA), dimethoxyethane (DME) and acetonitrile (ACN)

Compound	Solvent	λ_{abs}[a], nm	ε[b], M^{-1} cm^{-1}	λ_{fl}[c], nm	QY[d]
1	EA	297		357	0.10
	DME	298		357	0.07
	ACN	251, 298	26 103, 15 766	358	0.18
2	EA	306		386	0.01
	DME	306		408	0.02
	ACN	244, 306	47 681, 22 568	435	0.03
3	EA	323		441	0.18
	DME	256, 323		386, 443[e]	0.20
	ACN	257, 321	43 396, 14 819	393, 490[e]	0.17
4	EA	288, 363		436, 585[e]	0.05
	DME	289, 363		452, 603[e]	0.02
	ACN	290, 364	31 929, 6264	513, 653[e]	0.001

[a] Absorption maxima. [b] Molar extinction coefficients at wavelengths of absorption maxima. [c] Fluorescence maxima, obtained by excitation of compounds **1** and **2** at 300 nm, **3** at 320 nm and **4** at 360 nm. [d] Quantum yields were determined by the comparative method relative to 9,10-diphenyl anthracene in cyclohexane. [e] Dual fluorescence peak wavelengths were obtained by fitting emission spectra with the Gaussian peak function

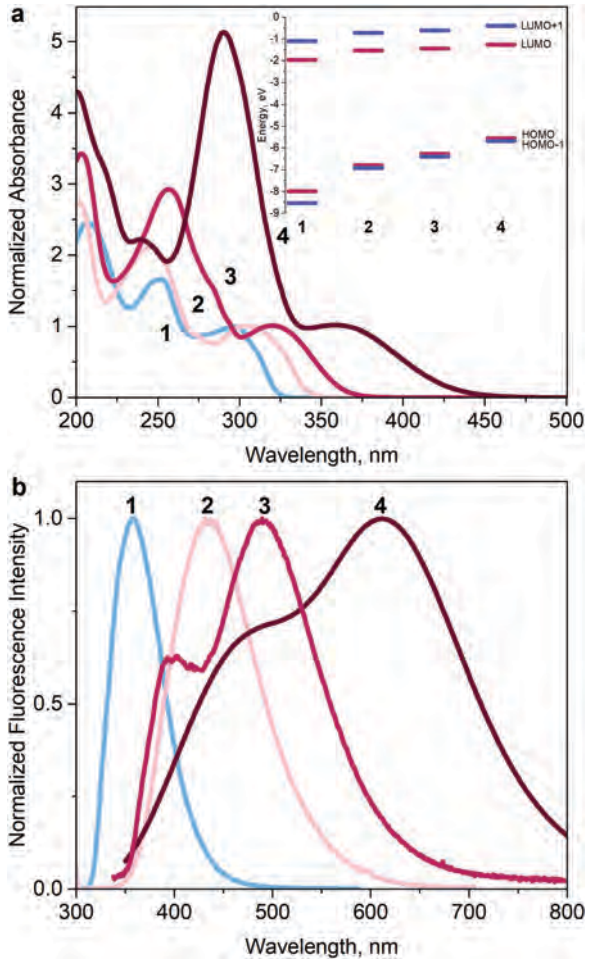

Fig. 2 (a) Absorption spectra normalized to maxima of red side absorption bands of compounds **1** to **4** in ACN. The inset is a representative scheme of HOMO, HOMO−1, LUMO and LUMO+1 energies, obtained using the BMK functional at the 6-31g(d,p) basis set level in a vacuum. (b) Normalized fluorescence spectra of **1** to **4** in ACN (10^{-5} M). The represented fluorescence spectrum of **4** is a two Gaussian peak function fit of the experimental spectrum

along with positive solvatochromism in other solvents also observed in similarly modified 2,4-bis(triazolyl) pyrrolo[2,3-*d*]pyrimidines.[15] The most impressive emission feature is present in compounds **3** and **4**, as the incorporation of strong electron donors results in dual fluorescence. In the case of **3**, two CT emission bands are observed in DME and ACN, while for **4**, dual CT emission was recorded in all of the three tested solvents along with more explicit spectral separation between fluorescence bands. It is evident that the dual character of fluorescence is enhanced with increased electron donating ability of substituents as well as increased polarity (dielectric constant) of solvents.

Time-resolved fluorescence experiments in ACN show that both emitting states have their characteristic fluorescence decay transients and should be fitted separately (see Fig. 3 for **3** and **4**). For instance, the blue side emission of compound **3** has a lifetime of 2.41 ns, while the red side – 4.4 ns.

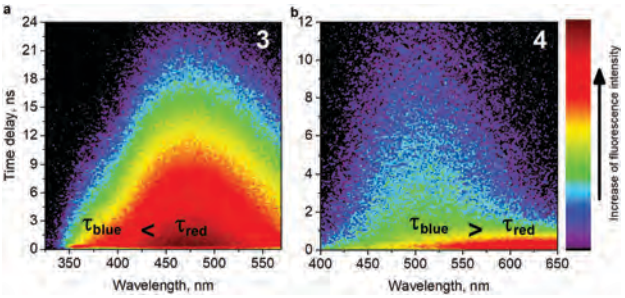

Fig. 3 Time-resolved fluorescence maps of compounds **3** (a) and **4** (b) in ACN (10^{-5} M).

More unusual behaviour is observed for compound **4** as the emission lifetime at the blue side of spectra (6 ns) is longer than the red one (2.71 ns). The latter behaviour (of compound **4** fluorescence decay) suggests that both CT states might be independent of each other.

Many examples of organic molecules exhibiting dual fluorescence can be found in the literature. Most commonly, for donor–acceptor systems two fluorescence bands are attributed to emission from the LE states, which occurs in the (near) Franck–Condon region, while the low-energy emission is mostly referred to the CT state, accompanied by excited-state structural relaxation and charge re-distribution.[36] The CT states can also be classified into several other states like the twisted internal charge transfer (TICT)[37–39] and planar internal charge transfer (PICT)[38] states that depend on the molecular configuration. However, to all in common, CT states are usually inaccessible by direct excitation, and thus can only be formed from the LE state and therefore exhibit fluorescence at longer wavelengths with longer fluorescence lifetimes.[36] Usually, fluorescence from the LE state does not depend on solvent polarity, while, on the contrary, because of molecule being more polar in the CT state, strongly red-shifted or broaden CT emission spectra are often observed.[37] In the present case, both the emitting states of **3** and **4** are solvent dependent, with the red side emitting species being more polar. Additionally, ''pure'' LE-like spectra of compound **1** are in the deep blue region, peaking at 357–358 nm. As the observed blue side fluorescence for **3** and **4** is already shifted to longer wavelengths by at least 30 nm, the origin of the dual emission of studied compounds is from two CT states.

Several unusual cases of the dual emission from two CT states have already been shown; however, each case is specific. For example, for the D–A–D′ systems (which can be successfully applied for the third generation organic light emitting diodes) two CT states of one molecule have been attributed to both intramolecular CT and intermolecular CT, caused by exciplex emission,[6] or to different conformers of the D–A–D′ system.[7] Additionally, it was shown that two transitions are possible from D and D′ fragments.[40] Furthermore, it was discovered that two independent CT emitting states can exist in one molecular system and can be attributed to D–A and A–D′ moieties and are controlled by conformations and stabilized by the polarity of the surroundings.[8]

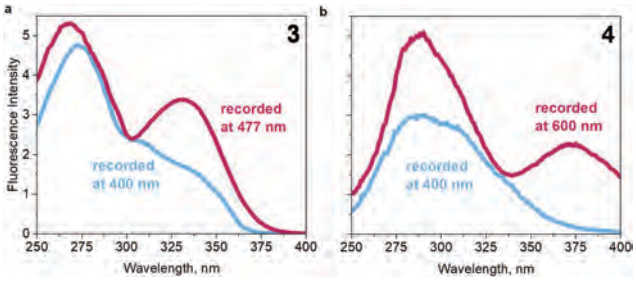

Fig. 4 Excitation spectra of **3** (a) and **4** (b) recorded in ACN (10^{-5} M) at different wavelengths – 400 nm and 477 nm for **3**; 400 nm and 600 nm for **4**.

To further prove the independent origin of the observed CT emission bands in the current work, excitation spectra were recorded for **3** and **4** (Fig. 4). States responsible for the blue and red side emissions have different excitation spectra. The red emission is related to the lowest absorption CT states (>325 nm (**3**), >360 nm (**4**)), while the blue emission corresponds to higher excited states (*ca.* 310 nm (**3**) and *ca.* 330 nm (**4**)). Thus the origin of the dual CT emission may be assigned to an interplay of charge transfer between one of the electron donating branches and bis-triazolyl-purine as an acceptor in separate molecules, which is a unique feature of asymmetric D–A–D′ systems.[7,8]

According to electron density distribution in HOMO – LUMO and HOMO−1 – LUMO (Fig. 5a), we attribute the blue emission to transition within the C2 branch (for further simplification, we name it a "blue" branch), while the red side band of emission is caused by charge transfer in the C6 branch (a "red" branch). See Fig. 5b for the representative fluorescence spectra for both transitions.

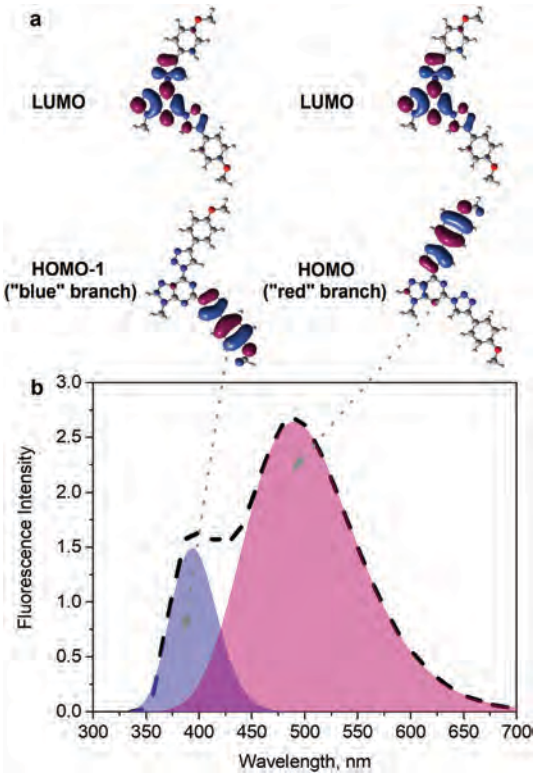

Fig. 5 (a) Spatial distribution of HOMO – LUMO and HOMO−1 – LUMO molecular orbitals of compound **3**, obtained using a BMK functional with a 6-31g(d,p) basis set in a vacuum. (b) The contribution of emission caused by distinct charge transfer to the fluorescence spectra of **3** in ACN. The dashed line represents the experimental spectrum. The filled blue and red emission spectra were obtained by spectral deconvolution, performed with the two Gaussian peak function.

Fluorescence ratiometric chemical sensor

In the current work, the uncommon molecular feature of the dual independent emission of the D–A–D′ asymmetric compound was exploited for the creation of a ratiometric chemical sensor, since the change of the intensity ratio between two fluorescence peaks in the presence of analytes is an operating principle of a self-calibrating sensor.[41–43] Here we combine the selective bonding and the dual nature of the fluorescence to create a fluorescence sensor based on a purine D–A–D′ system. We further selected compound **3** as the best candidate for cation sensor due to its highest fluorescence QYs (around 20%) along with a sufficient spectral separation between fluorescence bands in ACN.

Steady-state absorption and fluorescence titration experiments were performed using alkali (Na^+ and K^+), alkaline earth (Ca^{2+}) and transition (Fe^{2+}, Cu^+, Zn^{2+}) metal ions . The steady-state absorption spectra upon titration with cations remained almost unchanged. However, the main changes upon complexation with metal ions are observed in the fluorescence spectra, where the blue side emission is completely quenched (Fig. 6a). The dependence of the fluorescence intensity at 400 nm on the equivalents of Zn^{2+} and Ca^{2+} upon titration is shown in Fig. 6a inset , which implies another appealing fact that complexation at room temperature occurs between one metal ion and three to five purine molecules. The interaction of **3** with metal ions leads to only negligible changes of the "red" branch emission at 500 nm, most probably due to the specific site of coordination of each metal ions. It is worth noting that **3** was not sensitive to alkali metal ions (Na^+ and K^+).

The NMR titration experiments of compound **3**, performed using $Ca(ClO_4)_2{\cdot}4H_2O$ and $Zn(ClO_4)_2{\cdot}6H_2O$ in CD_3CN at 50 °C , prove the complexation with the equivalence point reached at the purine : M^{2+} ratio of 3 : 1. Interestingly, changes of the chemical shift ($\Delta\delta$) during titration with Ca^{2+} and Zn^{2+} salts showed different patterns. With calcium perchlorate the largest $\Delta\delta$ values were observed for H–C5′ of both triazoles, whereas with zinc perchlorate the purine H-C8 and one of the triazoles H–C5′ underwent the largest shift. This indicates that Ca^{2+} is coordinated between both triazoles, while Zn^{2+} complexes between the triazole at C6 and N7 of the purine (Fig. 6b and c). The coordination and its pattern with Zn^{2+} ions was additionally proved by the NMR titration experiments with a model compound, bearing a sole triazole substituent at C6 . The latter molecule revealed an identical complexation pattern (chemical shift change) as compound **3** . In fact, compounds **2** and **4** also form the same

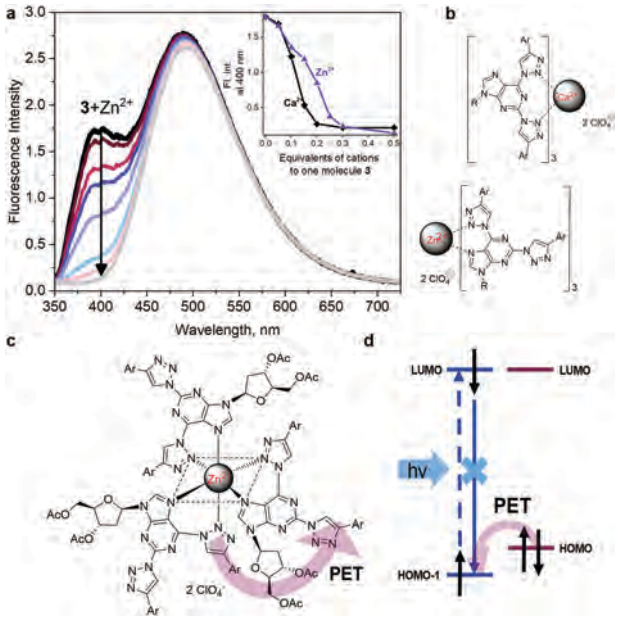

Fig. 6 (a) The fluorescence titration experiment of compound **3** (10^{-5} M) upon addition of Zn^{2+} metal ions from 0 to 0.5 equivalents in ACN; inset – the dependence of the fluorescence intensity at 400 nm on the equivalents of Ca^{2+} and Zn^{2+} metal ions. (b) The suggested complexation mode of compound **3** to Ca^{2+} and Zn^{2+} salts based on NMR titration results, where Ar = 4-methoxyphenyl; R = 3′,5′-di-*O*-acetyl-2′-deoxy-β-D-ribofuranosyl, and (c) the illustration of the purine – Zn^{2+} (3 : 1) octahedral complex. (d) The sensing mechanism of PET upon complexation with metal ions and excitation of the ''blue'' branch. The scheme represents PET occurring between two distinct molecules.

complexes with metal ions, confirming the generality of using bis-triazolyl purines as chemosensors .

So far, it is evident that the complexation of **3** with metal ions causes an assembly (''aggregation'') of several ligand molecules, along with complete quenching of the ''blue'' branch emission. In addition, metal ions do not induce changes of fluorescence lifetimes upon complexation . Therefore, three sensing mechanisms, related to intermolecular distances, should be considered – Förster resonance energy transfer (FRET), Dexter exchange energy transfer (EET) and PET. These processes should happen on a sub-picosecond time scale, similar to that reported for covalently bounded compounds.[44] Even if the essentials for FRET and EET are realized in our system (a close proximity between energy donor and acceptor and spectral overlap between acceptor absorption and donor emission[45,46]), these mechanisms were ruled out as no increase of the red fluorescence band intensity together with no changes of emission lifetimes were observed.

Thus, we suggest that upon interaction with cations, molecules pack closely with each other and in the case of the ''blue'' branch being excited, the intermolecular interbranch PET takes place. Importantly, estimated energies of HOMO and HOMO−1 are favorable for the latter process. This is an exceptional property of the D–A–D′ based system, determined by chemically identical, though assymetrically linked donor moeities. Fig. 6d summarizes the following suggested mechanism: the electron is transferred from the HOMO level of the unexcited molecule (''red'' branch) to the HOMO−1 of the excited one (''blue'' branch), thus the blue side emission is quenched.

To get a deeper insight into the mechanism of PET, we employed the transient absorption spectroscopy experiments. Two representative metal ions of Ca^{2+} and Zn^{2+} (0.5 equivalents of each) and compound **3** diluted in ACN were used in experiments, performed by excitation at 320 nm (both branches were excited) and 350 nm (only the ''red'' branch was excited). The results are presented in Fig. 7 .

To all samples in common, there are two main regions of the excited state absorption (ESA) that will be further referred to as region I (with spectral components named as **a** at 395 nm, **b** at 425 and **c** at 465 nm) and region II (*ca.* 600 nm). Starting from a few tens of picoseconds, the transient absorption spectra are the same for all samples and are similar to cation-radical absorption of anisole, peaking at 430 nm,[47] while the red side ESA at around 590 nm is analogous to the purine anion-radical absorption spectra.[48]

Once the samples are excited (at 320 nm or at 350 nm), the initial spectral feature at 465 nm (band **c**) evolves with an excitation pulse and may be attributed to the excited ligand of **3** or to the excited complexes of **3** with Ca^{2+} or Zn^{2+} in the ground state geometry. The relaxation of component **c** in a few hundred femtoseconds corresponds to the structural relaxation of the excited samples together with the rearrangement of surrounding solvent molecules. The transient absorption experiments on the compound **3** embedded in the PMMA matrix (frozen ground state geometry) show no spectral shifts of the band **c** even up to 10 ps delay .

If the samples are excited at 320 nm (both ''blue'' and ''red'' branches), two distinct peaks at *ca.* 395 nm (band **a**) and *ca.* 425 nm (band **b**) and the region II grow with the same time

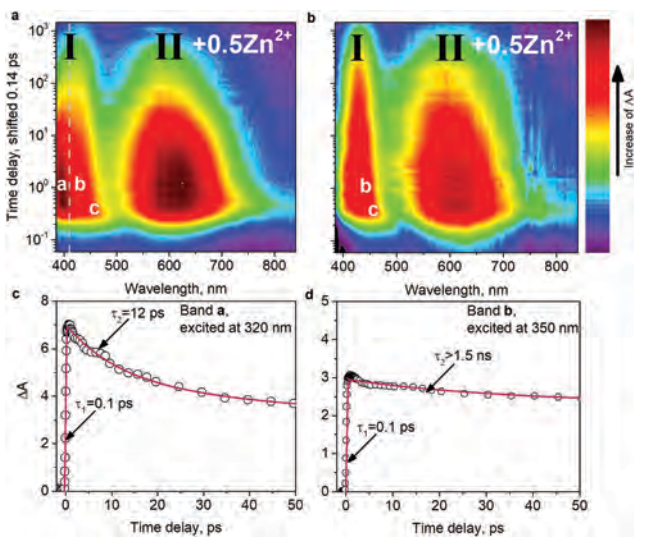

Fig. 7 Transient absorption maps of compound **3** with 0.5 equivalent of Zn^{2+} cations in ACN, obtained by excitation of the sample at (a) 320 nm and (b) 350 nm. The respective excited state absorption transients, fitted at (c) 395 nm and (d) at 425 nm. A slight overlap with band **c** is observed in kinetics (d), which produces a short and weak component at the beginning of decay.

constant of a few hundred femtoseconds corresponding to the lifetime of the band **c**. In the case of excitation at 350 nm (only the ''red'' branch), the band **a** is not present (Fig. 7b

During the relaxation of the band **c**, the formation of the radical pair with intermolecular electron transfer from the ''red'' chromophore ground state to the excited ''blue'' chromophore ground state occurs. The observed 12 ps decay of ESA, located at *ca.* 395 nm (band **a**) and 630–650 nm (region II), corresponds to the radical recombination time constant (Fig. 7a). It is worth noting that no signal increase with the time constant of 12 ps was observed in the entire experimental spectral range, indicating that neither FRET nor EET occurs in the present system.

Thus, the easily accessible modification of the purine ring allowed creation of a unique molecular structure with two chemically identical, though, asymmetrical electron donating branches linked through a triazole, which assists in the coordination with metal ions. This allowed us to realize the favorable conditions for the efficient PET – the energy difference between HOMO and HOMO−1 of each branche is small enough; in addition, the coordination with cations ensures the close proximity between those ''non-communicating'' branches. The further modification of triazoles as spacers and coordinating elements opens endless opportunities to selectively sense the desired analytes. On the other hand, the alteration of the electron donating moieties would provide possibilities for boosting sensitivity and combining the appropriate optical properties. The study in alcohols and water revealed a somewhat different behaviour of ligand **3** upon complexation; the upcoming article will be devoted to comprehensive investigations of photophysics and sensing mechanism of compounds **1–4** in protic environments.

Conclusions

In conclusion, we demonstrate the possibility of constructing a ratiometric fluorescence cation sensor based on the asymmetrically functionalized purine with electron donating groups. The observed dual-band fluorescence is produced by two non-communicating electronic transitions within the same ligand. PET occurs between D and D′ fragments of neighbouring ligands assembled upon complexation with metal ions and is responsible for the quenching of the blue fluorescence band. We believe that the reported strategy can be general for a wealth of D–A–D′ compounds across a wide spectral window and specific selectivity for chemical species, which can be further altered by the modification of spacers used for the coordination or electron donating substituents.

Conflicts of interest

There are no conflicts to declare.

Acknowledgements

This project has received funding from the European Social Fund (Project No. 09.3.3-LMT-K-718-01-0026) under a grant agreement from the Research Council of Lithuania (LMTLT) and from the Latvian Council of Science (Project No. LZP-2018/2-0037). The authors thank Kamile Tulaite for the help with sample preparation and optical measurements.

Notes and references

1 F. Bureš, *RSC Adv.*, 2014, **4**, 58826–58851.
2 S. Tang and J. Zhang, *J. Phys. Chem. A*, 2011, **115**, 5184–5191.
3 P. Gautam, R. Misra, S. A. Siddiqui and G. D. Sharma, *ACS Appl. Mater. Interfaces*, 2015, **7**, 10283–10292.
4 P. Sonar, S. P. Singh, P. Leclère, M. Surin, R. Lazzaroni, T. T. Lin, A. Dodabalapur and A. Sellinger, *J. Mater. Chem.*, 2009, **19**, 3228–3237.
5 Z. Chen, J. Yang, F. Wu, L. Chen and Y. Chen, *Chem. Res. Chin. Univ.*, 2017, **33**, 305–311.
6 R. Skaisgiris, T. Serevičius, K. Kazlauskas, Y. Geng, C. Adachi and S. Juršėnas, *J. Mater. Chem. C*, 2019, **7**(40), 12601–12609.
7 K.-L. Woon, C.-L. Yi, K.-C. Pan, M. K. Etherington, C.-C. Wu, K.-T. Wong and A. P. Monkman, *J. Phys. Chem. C*, 2019, **123**, 12400–12410.
8 M. Aydemir, S. Xu, C. Chen, M. R. Bryce, Z. Chi and A. P. Monkman, *J. Phys. Chem. C*, 2017, **121**, 17764–17772.
9 E. Tulyakova, S. Delbaere, Y. Fedorov, G. Jonusauskas, A. Moiseeva and O. Fedorova, *Chem. – Eur. J.*, 2011, **17**, 10752–10762.
10 P. Meti, J. W. Yang and Y. D. Gong, *Dyes Pigm.*, 2018, **156**, 233–242.
11 G. S. Collier, L. A. Brown, E. S. Boone, M. Kaushal, M. N. Ericson, M. G. Walter, B. K. Long and S. M. Kilbey, *J. Mater. Chem. C*, 2017, **5**, 6891–6898.
12 I. Novosjolova, E. Bizdena and M. Turks, *Eur. J. Org. Chem.*, 2015, 3629–3649.
13 L. Zilbershtein-Shklanovsky, M. Weitman, D. T. Major and B. Fischer, *J. Org. Chem.*, 2013, **78**, 11999–12008.
14 A. Šišuļins, J. Bucevičius, Y. T. Tseng, I. Novosjolova, K. Traskovskis, Ē. Bizdēna, H. T. Chang, S. Tumkevičius and M. Turks, *Beilstein J. Org. Chem.*, 2019, **15**, 474–489.
15 J. Bucevicius, L. Skardziute, J. Dodonova, K. Kazlauskas, G. Bagdziunas, S. Jursenas and S. Tumkevicius, *RSC Adv.*, 2015, **5**, 38610–38622.
16 J. Bucevicius, M. Turks and S. Tumkevicius, *Synlett*, 2018, 525–529.
17 R. S. Butler, A. K. Myers, P. Bellarmine, K. A. Abboud and R. K. Castellano, *J. Mater. Chem.*, 2007, **17**, 1863–1865.
18 Y. Yang, P. Cohn, A. L. Dyer, S. H. Eom, J. R. Reynolds, R. K. Castellano and J. Xue, *Chem. Mater.*, 2010, **22**, 3580–3582.
19 Y. Yang, P. Cohn, S. H. Eom, K. A. Abboud, R. K. Castellano and J. Xue, *J. Mater. Chem. C*, 2013, **1**, 2867–2874.

20 Z. Wang, J. Yao, L. Zhan, S. Gong, D. Ma and C. Yang, *Dyes Pigm.*, 2020, 108437.

21 K. M. Sun, C. K. McLaughlin, D. R. Lantero and R. A. Manderville, *J. Am. Chem. Soc.*, 2007, **129**, 1894–1895.

22 V. Venkatesh, A. Shukla, S. Sivakumar and S. Verma, *ACS Appl. Mater. Interfaces*, 2014, **6**, 2185–2191.

23 J. Li, Y. Zhang, H. Zhang, X. Xuan, M. Xie, S. Xia, G. Qu and H. Guo, *Anal. Chem.*, 2016, **88**, 5554–5560.

24 S. H. Gao, M. S. Xie, H. X. Wang, H. Y. Niu, G. R. Qu and H. M. Guo, *Tetrahedron*, 2014, **70**, 4929–4933.

25 J.-P. Li, H.-X. Wang, H.-X. Wang, M.-S. Xie, G.-R. Qu, H.-Y. Niu and H.-M. Guo, *Eur. J. Org. Chem.*, 2014, 2225–2230.

26 A. Dumas and N. W. Luedtke, *Chem. – Eur. J.*, 2012, **18**, 245–254.

27 A. Omumi, C. K. McLaughlin, D. Ben-Israel and R. A. Manderville, *J. Phys. Chem. B*, 2012, **116**, 6158–6165.

28 Z. Dong, W. Chen, H. Li, Y. Dai, T. Zheng, H. Zhang, H. Xu and H. Lu, *Inorg. Chem. Commun.*, 2020, **116**, 107915.

29 G. Wu, Z. Wang, W. Zhang, W. Chen, X. Jin and H. Lu, *Inorg. Chem. Commun.*, 2019, **102**, 233–239.

30 H.-Y. Xu, W. Chen, W. Zhang, L. Ju and H. Lu, *New J. Chem.*, 2020, **44**, 15195–15201.

31 K. Ozols, D. Cīrule, I. Novosjolova, D. Stepanovs, E. Liepinsh, Ē. Bizdēna and M. Turks, *Tetrahedron Lett.*, 2016, **57**, 1174–1178.

32 D. Cīrule, K. Ozols, O. Platnieks, Ē. Bizdēna, I. Māliņa and M. Turks, *Tetrahedron*, 2016, **72**, 4177–4185.

33 A. Kovaļovs, I. Novosjolova, Ē. Bizdēna, I. Bižāne, L. Skardziute, K. Kazlauskas, S. Jursenas and M. Turks, *Tetrahedron Lett.*, 2013, **54**, 850–853.

34 C. Dyrager, K. Börjesson, P. Dinér, A. Elf, B. Albinsson, L. M. Wilhelmsson and M. Grøtli, *Eur. J. Org. Chem.*, 2009, 1515–1521.

35 R. S. Butler, P. Cohn, P. Tenzel, K. A. Abboud and R. K. Castellano, *J. Am. Chem. Soc.*, 2009, **131**, 623–633.

36 J. R. Lakowicz, *Principles of Fluorescence Spectroscopy*, Springer, 3rd edn, 2006.

37 S. Sasaki, G. P. C. Drummen and G. Konishi, *J. Mater. Chem. C*, 2016, **4**, 2731–2743.

38 Z. R. Grabowski and K. Rotkiewicz, *Chem. Rev.*, 2003, **103**, 3899–4031.

39 Z. R. Grabowski, K. Rotkiewicz and A. Siemiarczuk, *J. Lumin.*, 1979, **18–19**, 420–424.

40 A. Tomkeviciene, T. Matulaitis, M. Guzauskas, V. Andruleviciene, D. Volyniuk and J. V. Grazulevicius, *Org. Electron.*, 2019, **70**, 227–239.

41 Z. Liu, W. He, Z. Guo, M. Schmittel, P. Aneesa, A. Ajayaghosh, W. Guo, J. Kim, S. Park, J. Yoon and Z. Zeng, *Chem. Soc. Rev.*, 2013, **42**, 1568.

42 X. Zhang, Y. Xiao and X. Qian, *Angew. Chem., Int. Ed.*, 2008, **47**, 8025–8029.

43 J. F. Zhang, Y. Zhou, J. Yoon, Y. Kim, S. J. Kim and J. S. Kim, *Org. Lett.*, 2010, **12**, 3852–3855.

44 P. A. Panchenko, Y. V. Fedorov, O. A. Fedorova and G. Jonusauskas, *Phys. Chem. Chem. Phys.*, 2015, **17**, 22749–22757.

45 I. Medintz and N. Hildebrandt, *FRET – Förster Resonance Energy Transfer: From Theory to Applications*, 2013.

46 S. Faure, C. Stern, R. Guilard and P. D. Harvey, *J. Am. Chem. Soc.*, 2004, **126**, 1253–1261.

47 P. O'Neill, S. Steenken and D. Schulte-Frohlinde, *J. Phys. Chem.*, 1975, **79**, 2773–2779.

48 P. N. Moorthy and E. Hayon, *J. Am. Chem. Soc.*, 1975, **97**, 3345–3350.